A PENELOPE-based system for the automated Monte Carlo simulation of clinacs and voxelized geometries—application to far-from-axis fields

Josep Sempau[a)]
Institut de Tècniques Energètiques, Universitat Politècnica de Catalunya, Diagonal 647, E-08028 Barcelona, Spain

Andreu Badal
Division of Imaging and Applied Mathematics, OSEL, CDRH U.S. Food and Drug Administration, 10903 New Hampshire Ave, Silver Spring, Maryland 20993-0002

Lorenzo Brualla
NCTeam, Strahlenklinik, Universitätsklinikum Essen, Hufelandstr. 55, D-45122 Essen, Germany

(Received 8 June 2011; revised 17 August 2011; accepted for publication 4 September 2011; published 11 October 2011)

Purpose: Two new codes, penEasy and penEasyLinac, which automate the Monte Carlo simulation of Varian Clinacs of the 600, 1800, 2100, and 2300 series, together with their electron applicators and multileaf collimators, are introduced. The challenging case of a relatively small and far-from-axis field has been studied with these tools.

Methods: penEasy is a modular, general-purpose main program for the penelope Monte Carlo system that includes various source models, tallies and variance-reduction techniques (VRT). The code includes a new geometry model that allows the superposition of voxels and objects limited by quadric surfaces. A variant of the VRT known as particle splitting, called fan splitting, is also introduced. penEasylinac, in turn, automatically generates detailed geometry and configuration files to simulate linacs with penEasy. These tools are applied to the generation of phase-space files, and of the corresponding absorbed dose distributions in water, for two 6 MV photon beams from a Varian Clinac 2100 C/D: a 40×40 cm^2 centered field; and a 3×5 cm^2 field centered at (4.5, -11.5) cm from the beam central axis. This latter configuration implies the largest possible over-traveling values of two of the jaws. Simulation results for the depth dose and lateral profiles at various depths are compared, by using the gamma index, with experimental values obtained with a PTW 31002 ionization chamber. The contribution of several VRTs to the computing speed of the more demanding off-axis case is analyzed.

Results: For the 40×40 cm^2 field, the percentages γ_1 and $\gamma_{1.2}$ of voxels with gamma indices (using 0.2 cm and 2% criteria) larger than unity and larger than 1.2 are 0.2% and 0%, respectively. For the 3×5 cm^2 field, $\gamma_1 = 0\%$. These figures indicate an excellent agreement between simulation and experiment. The dose distribution for the off-axis case with voxels of $2.5 \times 2.5 \times 2.5$ mm^3 and an average standard statistical uncertainty of 2% (1σ) is computed in 3.1 h on a single core of a 2.8 GHz Intel Core 2 Duo processor. This result is obtained with the optimal combination of the tested VRTs. In particular, fan splitting for the off-axis case accelerates execution by a factor of 240 with respect to standard particle splitting.

Conclusions: penEasy and penEasyLinac can simulate the considered Varian Clinacs both in an accurate and efficient manner. Fan splitting is crucial to achieve simulation results for the off-axis field in an affordable amount of CPU time. Work to include Elekta linacs and to develop a graphical interface that will facilitate user input is underway. © *2011 American Association of Physicists in Medicine*. [DOI: 10.1118/1.3643029]

Key words: penelope, penEasy, penEasyLinac, voxelized geometry

I. INTRODUCTION

An important application of the Monte Carlo (MC) method in medical physics is the characterization of radiation fields produced by linear accelerators (linacs) used in radiotherapy treatments.[1,2] The accurate simulation of a linac requires a detailed description of its geometry and, depending on the configuration, the application of elaborate variance-reduction techniques (VRTs) (Refs. 3 and 4) to produce reasonably low statistical uncertainties in an affordable amount of computing time.

The interpretation of linac blueprints and introduction of the geometry into the MC system can be a tedious and error-prone task. Furthermore, technical specifications provided by the manufacturers do not always contain all the relevant data.[5] The introduction of VRTs, in turn, may require modification of the computer code and this can involve a substantial programming effort by the end user. Since most general-

purpose main programs usually distributed with MC packages are not specifically designed for this context, adaptations or extensions of existing codes have been developed by various authors to facilitate the users' work. BEAM (Ref. 6) and BEAMnrc (Ref. 7), based on the widely known EGS4 (Ref. 8) and EGSnrc codes (Refs. 9 and 10), respectively, are examples of this approach.

Here, we introduce two new codes, named PENEASY and PENEASYLINAC, which together allow the automated and efficient MC simulation of radiation fields, and the corresponding dose distributions in the patient, produced by several Varian[11] Clinacs. PENEASY is essentially a general-purpose main program for the PENELOPE (Refs. 12 and 13) MC system. Among other features, it introduces the possibility of simulating geometries defined with a regular grid of homogeneous cuboids (voxels) which, in medical applications, can be obtained from a computerized tomography (CT) scan. The second code, PENEASYLINAC, automatically generates input files for PENEASY for any selected configuration of the linac.

A demanding test for a linac simulator is the computation of absorbed dose distributions produced by relatively small far-from-axis photon fields. The accurate description of these configurations is essential for the dosimetry of some radiotherapy techniques based on narrow or composite nonstandard fields, such as intensity modulated radiation therapy, where several small fields are used, many of them off-axis, with different intensities and with various angles of incidence on the patient. A new international formalism to standardize their dosimetry has been proposed under the auspices of the International Atomic Energy Agency (IAEA) in cooperation with other organizations.[14] Tools such as those presented in this work will be useful for the evaluation of the correction factors required for the application of these new dosimetry protocols.

The rest of the paper is organized as follows. A short description of the features of the new codes is given in Sec. II. Details about a newly developed VRT and a new algorithm for voxelized geometries are also given in this section. Experimental measurements and PENEASYLINAC simulations for a far-from-axis field are compared in Sec. III, which includes an analysis of the performance of the applied VRTs. Finally, conclusions are drawn in Sec. IV.

II. PENEASY AND PENEASYLINAC

The PENELOPE package contains subroutines to describe the coupled transport of photons, electrons and positrons in material systems limited by quadric surfaces (planes, cylinders, cones, spheres, etc.) Photons are simulated following a detailed procedure, in other words, their interactions are followed in chronological succession one by one. For charged particles, detailed simulation is only feasible at relatively low energies, when the number of interactions per history is moderate. To accelerate the simulation, a mixed simulation scheme which distinguishes between hard and soft events is adopted for electrons and positrons. In this approach, hard events, defined as those involving angular deflections or energy losses above certain cutoffs, are simulated in a detailed way. All soft collisions encountered between two hard interactions are lumped together and they are described by a single artificial event, sometimes referred to as the "hinge." The cutoffs are determined by five user-defined transport parameters: C1 and C2 control the cutoff for elastic collisions; WCC and WCR are the cutoffs for inelastic and bremsstrahlung interactions, respectively; and DSMAX is an upper limit for the step length. All particles are transported until their kinetic energies fall below certain user-defined absorption energies Eabs. In PENELOPE, users are responsible for writing a steering main program that defines the source of particles, the quantities of interest to be scored and the VRTs to be applied. Examples of main programs are included in the distribution.

The new code PENEASY, which is both free[15] and open source, provides a general-purpose modular main program for PENELOPE. The implemented source models cover a wide range of spatial and energy distributions: point-like and Gaussian-distributed sources in space, volumetric sources and radiation beams with arbitrary (quadric) shapes, Gaussian-distributed spectra and piece-wise continuous spectra, photon beams with arbitrary polarization and phase-space files (PSF). The considered tallies are spatial distributions (Cartesian, cylindrical, and spherical) of absorbed dose, pulse height spectra, fluence spectra, particle counters, PSFs in a given region of space and particle tracks.

The absorbed dose is obtained as the quotient between the energy deposited in a given region and its mass. The energy deposited is estimated by adding the energy lost by each particle in all interactions that occur inside the considered region. Notice that the consistent use of mixed simulation[12] implies that all interactions, either hard or artificially produced at a hinge to account for the combined effect of soft collisions, are precisely located in space. When, as a result of an interaction, a secondary particle is created, it is stored in a stack. All secondaries are processed in succession after the primary has been completed and, when a secondary particle is retrieved from the stack, its energy (kinetic energy in the case of an electron) is subtracted from the counter before its transport begins. Therefore, at the end of the simulation, the counter contains the deposited energy that has not been transferred to secondary particles. The energy deposited by electrons and positrons can alternatively be estimated by adding the products of the restricted stopping power, averaged along a step (between two consecutive hard interactions), and the length of that step. The deposited energy is then obtained as the sum of these products and the track-ends.[16] The computation of the deposited energy using this latter method is reported by the same tally that produces the fluence spectrum.

A geometry model capable of accommodating objects described in terms of quadric surfaces, voxels, or a superposition of both has also been developed for PENEASY. The quadric geometry is handled by invoking PENELOPE's standard geometry package, called PENGEOM. Tracking across voxels relies on a set of transport routines named PENVOX. A description of the main features of this new model is given in Sec. II B. For more details on the operation and inner workings of PENEASY the reader is referred to the documentation included in the distribution.

As mentioned earlier, penEasy is a general-purpose code. penEasyLinac, an evolution of the AutolinaC code described by Brualla *et al.*,[17] is a complementary tool that generates the input files required for the simulation of certain linacs with penEasy. Its current version includes all Varian Clinacs of the 600, 1800, 2100, and 2300 series, together with their electron applicators and multileaf collimators (MLC). Special care has been devoted to describing all the relevant geometric details, including an elaborate quadric model of the secondary collimator and the modifications on the primary collimator identified by Chibani and Ma.[5] These are essential for reproducing lateral profiles for 18 MV beams and large field sizes.[18] Material compositions and mass densities were defined according to the manufacturer's documentation.

To operate the code, users must prepare an input file where the linac model and its configuration are defined. The configuration is determined by whether the machine is operated in electron or photon mode, the nominal beam energy, the positions of the jaws and the position of each leaf of the MLC (or electron applicator size in electron mode). Based on these choices, the code creates a quadric geometry file for pengeom and a configuration file for penEasy defining the particle source, the values of penelope's transport parameters and the values of the parameters governing the applied VRTs. Notice that users can edit these (ASCII text) files and modify any parameter before running the penEasy simulation. In particular, the code sets the initial energy of the (monoenergetic) electron beam associated to each nominal energy based on comparisons between experimental data and simulations performed by the authors. Users may be interested, however, in using different values to better match the dose distributions produced by their machines.

penEasyLinac instructs penEasy to output a PSF, which contains the dynamical variables of all the particles that reach a scoring plane located just after the last linac element and above the patient surface. In a second stage, users can use this PSF as a radiation source for penEasy and compute absorbed dose distributions for the patient.

The structure of the overall system is represented in Fig. 1. The uppermost layer (named primo), still under development, will integrate the operation of all subsystems in a single graphical user interface.

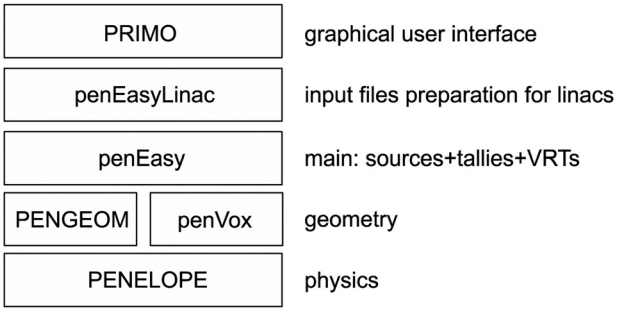

Fig. 1. Diagram showing the hierarchy of the various parts of the simulation system. Upper blocks rely on, or process data for, the routines contained in those located beneath them. primo is still under development.

II.A. Variance-reduction techniques

penEasy incorporates the following VRTs: interaction forcing, Russian roulette and particle splitting methods. Interaction forcing and Russian roulette are described in detail in the penelope manual.[12]

Regarding particle splitting, the code offers several modalities, depending on the degree of symmetry of the problem. In standard particle splitting, a particle that enters a region of space where it has a significant probability of contributing to the tally is replicated K times, with each identical replica having a statistical weight equal to $1/K$. No symmetry is needed to apply this method, and its efficacy (or lack of) largely depends on the strategy adopted to decide when it is to be applied and on the value of K.

A more elaborate method is rotational particle splitting, which can be applied when the object and the radiation source exhibit cylindrical symmetry. This is the case of the Varian Clinacs from the source down to the inclined mirror. In this technique, the kth replica ($k=1,\ldots,K$) of the primary particle is rotated an angle $2\pi k/K$ rad about the axis of symmetry. Rotational splitting is a simpler, and slightly more efficient, version of the azimuthal particle redistribution technique.[19] Although rotational splitting speeds up linac simulations of small centered fields, its usefulness is limited for far-from-axis fields such as those studied below. For these situations, a new technique, which will be referred to as fan splitting, is introduced here. Although the method is general, we shall describe it here within the context of linac simulation for concreteness and, also, to show how penEasyLinac takes advantage of it.

Fan splitting consists of cloning particles within an annular sector covering the considered off-axis field. For the particular case of Varian Clinacs, we have placed the splitting plane at 19 cm from the primary electron source. At this height in the gantry, particles have only traveled through a cylindrically symmetric geometry. Figure 2 shows a sketch of this plane in a beam's eye view, with the center of the

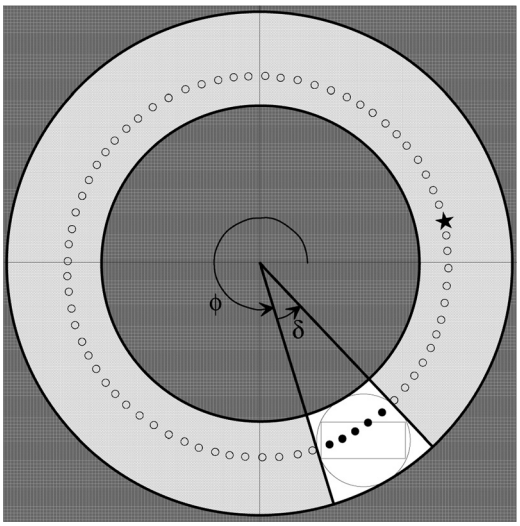

Fig. 2. Sketch showing the structure of the splitting plane. Details on the application of the fan splitting technique are given in the text.

cross-hair indicating the beam central axis and the rectangle in the fourth quadrant representing the off-axis field projected onto the splitting plane. An auxiliary circumference circumscribing the projected field is also drawn; the considered sector is defined in such a way that it completely covers it. The splitting plane is thus divided into three different regions depicted white (the annular sector), light grey, and dark grey in Fig. 2. To accurately describe the penumbras, margins of 3° and 3 cm (at 100 cm from the source) are allowed for the angles of the rays and the radii of the concentric circumferences limiting the white region, respectively.

Particles impinging on the dark grey region undergo a Russian roulette. A particle is discarded with probability, $\mathcal{P}$, and, if it survives, it is allowed to continue with a statistical weight augmented by a factor $1/(1-\mathcal{P})$. Each particle arriving at the white or light grey regions is rotationally split in K' replicas (empty dots, solid dots, and star) in such a way that a predetermined number K of them (solid dots) fall within the white region. The statistical weight of all the replicas is decreased by a factor $1/K'$. The K particles in the white region (solid dots), i.e., those located within and in the surroundings of the radiation field, are transported downstream from the splitting plane, as usual. As for the remaining $K'-K$ particles that fall within the less "interesting" light grey region, they are all discarded except for one. This only-surviving particle is chosen at random (represented by the star in Fig. 2) and, to keep the simulation unbiased, a factor $(K'-K)/K'$ is applied to its original statistical weight.

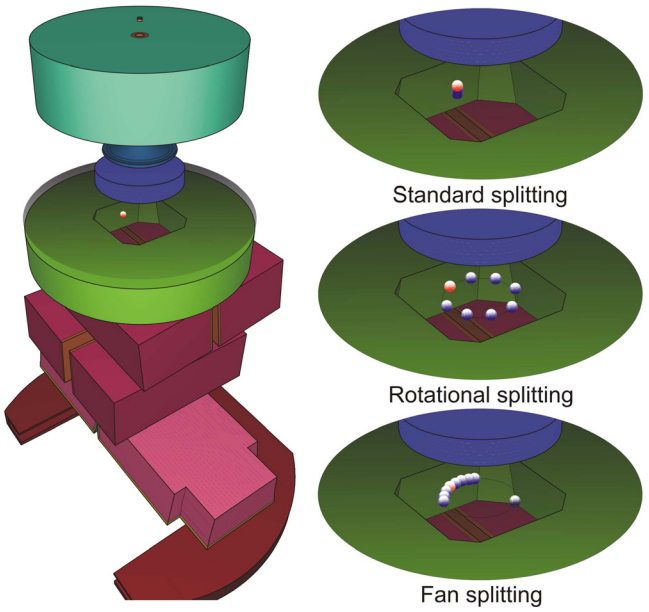

FIG. 3. On the left, a three-dimensional view of the Varian Clinac 2100 C/D geometry operating in photon mode is shown. The jaws are positioned to deliver the off-axis field discussed in Sec. III. Particle splitting is performed on the circular semitransparent plane located between the ionization chamber and the secondary collimator. The images on the right show a close-up of this plane in which the three splitting techniques are schematically depicted. A particle arriving at this plane is shown on the left. In the uppermost sketch on the right (standard splitting) the replicated particles appear superimposed to the original particle. In the other two cases (rotational splitting and fan splitting), the replicated particles are drawn around a circumference to illustrate their spatial distribution.

Figure 3 shows a 3D view of a linac head geometry produced by PENEASYLINAC together with a schematic representation of the three variants of the particle splitting technique discussed above. Unless simple splitting is requested by the user, fan splitting is applied when the central axis is outside the auxiliary circumference circumscribing the radiation field. If that is not the case, then rotational splitting is used. The code creates the corresponding input files for PENEASY.

To further improve efficiency, PENEASY includes still another splitting method termed xy splitting, applicable only when the object shows symmetry under the transformation of Cartesian coordinates $x \to -x$ and $y \to -y$. When this VRT is activated, four replicas with Cartesian coordinates (x,y), $(-x,y)$, $(x,-y)$ and $(-x,-y)$ are created with a statistical weight reduced by a factor of 0.25. PENEASYLINAC is prepared to take advantage of this technique since, downstream from the jaws, Varian Clinacs show the required four-fold symmetry.

PENEASYLINAC sets the VRT parameters (e.g., the splitting factor K or the survival probability for Russian roulette) for each case to reasonable values. These were optimized by means of a limited set of preliminary runs. It is possible, however, that for certain linac configurations better combinations exist. In any case, users can modify the input files for PENEASY to override the default PENEASYLINAC values.

To speed up the computation, PENEASYLINAC also relies on a technique termed movable-skins,[17] which consists of considering certain collimating elements of the linac as formed by skin and nonskin zones. Regions where particles are likely to emerge and contribute to beam contamination are defined as skins and their transport parameters and absorption energies are set to relatively low values so as to ensure that transport is performed to high accuracy. Regions that will absorb nearly all entering particles are defined as nonskins and higher absorption energies are assigned to them in order to avoid a waste of computation time. The skin depth depends on the beam energy, and PENEASYLINAC automatically sets the position of the interfaces dividing both kinds of regions according to the linac configuration selected by the user.

Another convenient feature is the possibility of using these codes in conjunction with the package of Linux scripts CLONEASY,[20] which provides a simple, yet efficient, parallelization method based on the Secure Shell Protocol under Unix systems.

II.B. Voxelized geometries

The handling of a large number of bodies with different mass densities is impractical with PENGEOM and, therefore, a different model is introduced in PENEASY for the simulation of voxelized geometries. This model, provided by a set of routines called PENVOX, accepts a list of voxels as input, each one characterized by a material index (which univocally identifies a material in the PENELOPE system) and mass density. This information can be obtained for patients by processing CT scans to obtain the approximate chemical composition and density of each volume element.[21,22]

It is important to remark that the transport physics adopted in PENELOPE, which models the $e^{\pm}$ trajectory as a sequence of hard and soft events (see above) joined by free flights, is oblivious of the presence of boundaries separating voxels made of the same material. This is fully consistent with the transport mechanics adopted in the algorithm. Since, as noted above, the dose estimator involves the scoring of energy deposition events at well-defined spatial locations, the tallying of the absorbed dose in each voxel is trivial: each deposition is simply assigned to the voxel containing the interaction site. This avoids the need to truncate or shorten $e^{\pm}$ steps as they approach a surface separating voxels made of the same material. It also implies that the transport physics is not affected by the voxel size. This is in contradistinction to other charged particle transport algorithms which, unless special methods are applied to score the dose,[23,24] require stopping of the particle at each voxel boundary.

The only remaining issue is the tracking of straight trajectories across a voxelized geometry in an efficient manner. Implementation of the algorithm is inspired on that contained in the DPM code[25] and on the algorithm described by Amanatides and Woo[26] for ray tracing. Particles follow straight lines that may travel across several voxels with the same material composition. A particle stops when it enters a voxel of a different material, encounters a quadric surface (see below), experiences an interaction, or escapes from the material system. If an interaction occurs, the physics routines determine the energy loss, the new direction of flight and the distance to the next interaction.

To account for changes in density from voxel to voxel, PENVOX scales the remaining distance up to the next interaction with the inverse of the density of the voxel being traversed. This method is exact since the employed cross section models do not depend on the mass density. The only exception is $e^{\pm}$ inelastic collisions, which are affected by the density effect correction [see ICRU 37 (Ref. 27) and references therein]. Fortunately, the dependence on density is relatively small and can be safely neglected for most purposes; in water, for instance, the mass stopping power obtained using the PENELOPE model for inelastic collisions varies by less than 1% when the mass density changes by as much as 20%.

PENEASY also allows the superposition of both quadric and voxelized geometries, a feature that finds applications in many areas of medical physics. An example is the computation of the dose distribution inside a patient with an implanted brachytherapy source. A notional example of a geometry defined for this purpose is shown in Fig. 4 to illustrate the concept. It can also be used to model the hardware elements present in a treatment room (table, floor, walls, etc.) while the patient is being irradiated.

The superposition of both geometries is performed by considering an imaginary voxels bounding box (VBB), a parallelepiped that contains all the voxels specified by the user in an input file. The VBB is embedded within the quadric geometry, occupying the space of a certain body identified by the user in the quadrics input file. Transport in these superposed geometries proceeds by invoking either PENGEOM or PENVOX depending on whether the particle moves within the quadric geometry or in a voxel, respectively. When the particle is in a voxel that is partially covered by a quadric surface (voxels in contact with the exterior of the brachytherapy source in Fig. 4, for instance), the algorithm interrogates both geometries to determine the nearest intersection.

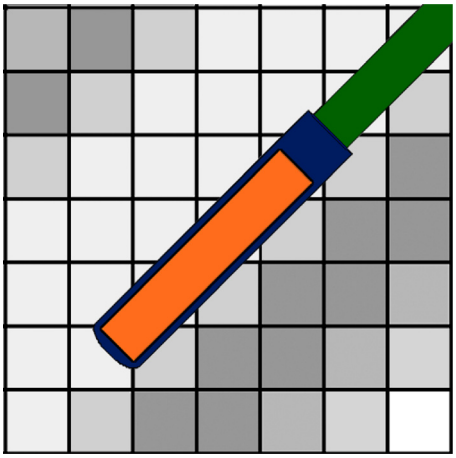

FIG. 4. A notional example of a superposition of voxels (a portion of a fictitious CT scan of a blood vessel) and quadrics (a brachytherapy source).

It should be pointed out that other authors have developed main programs to simulate voxelized geometries with PENELOPE.[28–30] However, to the best of our knowledge, none of them allows the combination of quadrics and voxels and is integrated in a modular code with a variety of source models and tallies as those found in PENEASY.

III. RESULTS

To illustrate the accuracy and performance of the PENEASY/PENEASYLINAC system, experimental data and simulation results have been compared for a 6 MV photon beam produced by a Varian Clinac 2100 C/D. The initial energy of the primary electrons, which is automatically set by the code, was 6.26 MeV. Transport parameters, also automatically selected, were set to different values for different elements of the linac. As an example, the absorption energies inside the skin of most collimating elements were 100 and 20 keV for charged particles and photons, respectively. The transport parameters C1, C2, WCC, and WCR were set to 0.1, 0.1, 100 keV, and 20 keV, respectively.

Our linac model was first validated by comparing the dose distribution produced in a water phantom for a centered field of 40×40 cm^2 with a source-to-surface distance (SSD) equal to 95 cm. In a first stage a PSF was generated and, in a subsequent simulation that used the PSF as a source, the dose distribution was computed on a grid of $0.5 \times 0.5 \times 0.5$ cm^3 voxels. A Cartesian reference system with its z axis along the central axis, pointing downstream, and the y axis along the direction of movement of the upper jaws was defined. The x direction coincides with the direction of movement of the leaves of the multileaf collimator. Experimental data were obtained with a PTW (Ref. 31) 31002 ion chamber. This is a cylindrical detector with a diameter of 5.5 mm, a height of 6.5 mm and an active volume of

154 mm^3. The chamber was placed with its longitudinal axis along the x direction and the diameter along the y direction.

Following Rogers and Mohan,[32] in PENEASY the average statistical uncertainty of a dose distribution is computed as the square root of the sum in quadrature of the estimated relative uncertainties in a subset of voxels. This subset contains voxels with a dose greater than half the maximum dose. In the plots that follow, MC uncertainties are of the order of magnitude or smaller than the symbol size use for the experiments and they will not be shown for clarity. Regarding experimental data, which were obtained as relative electrometer readings, their standard relative uncertainty is estimated to be 0.6%.[33] The (type B) uncertainty in the position of the detector is estimated to be 0.2 mm, and therefore, both experimental uncertainties are smaller than the symbol size and will not be plotted either.

A convenient measure of the agreement between two distributions is the gamma index.[34] The percentages γ_1 and $\gamma_{1.2}$ of voxels with a gamma value higher than 1 (not passing the test) and higher than 1.2 (manifestly beyond the acceptance limits), respectively, are the quantities reported hereafter as a measure of the degree of discrepancy. Only voxels with a dose larger than 10% of the dose maximum in the experimental data, which is taken as the reference data set, are considered. In our comparisons the dose difference (relative to the maximum) and distance-to-agreement (DTA) criteria are set to 2% and 0.2 cm, respectively.

The central axis depth dose distribution and lateral profiles are shown in Figs. 5(a) and 5(b), respectively. Relative experimental data have been scaled to match the (absolute, i.e., per history[35]) MC results as well as possible. The same scaling factor is used for all the data. As can be seen, agreement is very good, with values $\gamma_1 = 0.2\%$ and $\gamma_{1.2} = 0\%$. Similar results, not shown for brevity, are found for other configurations and Varian models.

We now turn our attention to the more interesting case of a far-from-axis field. The generation of PSFs for far-from-axis fields is a particularly delicate problem, since the majority of photons are likely to be absorbed by the jaws blocking their passage. Only a small fraction fall within the irradiated area and the analogue simulation becomes very inefficient, thus requiring extremely long computation times. In addition, particles inside the field travel at a slanted angle and a very detailed description of the edges of the jaws and of the secondary collimator is indispensable to reproduce the penumbras accurately.

Let us consider a 5×3 cm^2 6 MV photon beam centered at $x = 4.5$ cm, $y = -11.5$ cm and with a SSD equal to 100 cm. This implies that one of the X-jaws over-travels 2 cm and one of the Y-jaws over-travels 10 cm. These over-traveling values are the largest possible for the Varian 2100 C/D.

The same PTW 31002 chamber was used for the measurements. The depth dose distribution was obtained by positioning the chamber at the field center on the water surface and following a vertical path deep into the water. Note that, given the off-axis nature of the field, only the position at the surface was centered on the field. Dose lateral profiles were measured along x with $y = -11.5$ cm and along y with $x = 4.5$ cm, at depths $z = 1.4$, 5.0, 10.0, and 20.0 cm. As in the case of the reference field, a scaling factor, the same for all data, was applied to the experimental curves to match the MC results.

To take into account the detector volume effect, which is more prominent now than for the large centered field studied before due to the steeper gradient of the penumbras, the dose distribution was computed in water for a fine grid of voxels with a size of $0.05 \times 0.05 \times 0.1$ cm^3. To obtain the mean absorbed dose at each spatial location, this distribution was then summed over neighboring voxels occupying (approximately) the position that the chamber's air cavity would have if it were present. Admittedly, the comparison with experimental data is not rigorously correct, since for the latter the possible dependence of the chamber perturbation factors[33] on the irradiation conditions is disregarded. This is an approximation that, in view of the results presented below, seems to be acceptable at the uncertainty level reached in our study.

The depth dose distribution and lateral profiles along x and y are presented in Figs. 6–8, respectively. Agreement between experiment and simulation is excellent, with a value $\gamma_1 = 0\%$.

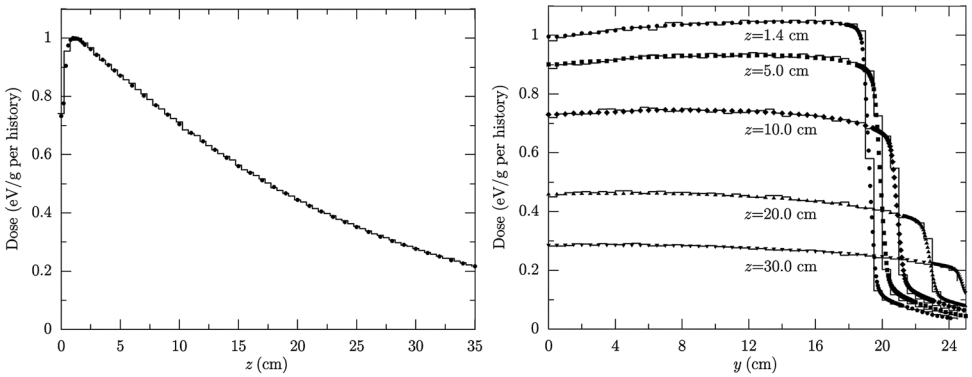

FIG. 5. Central axis depth dose (a) and lateral profiles (b) in water obtained for a 40×40 cm^2 reference field of 6 MV photons. Experimental data are shown with symbols and MC results are the histograms. Due to the symmetry of the field only half of the lateral profiles along the centered y axis are shown. The average relative standard statistical uncertainty of MC results is 1% (1σ).

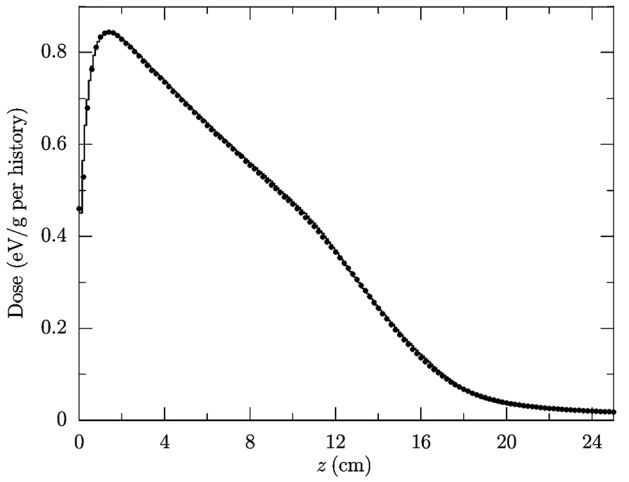

FIG. 6. Depth dose distribution for a 5×3 cm^2 off-axis field of 6 MV photons centered at $x = 4.5$ cm, $y = -11.5$ cm. Details are the same as in Fig. 5. The average relative statistical uncertainty of MC data is 0.1% (1σ).

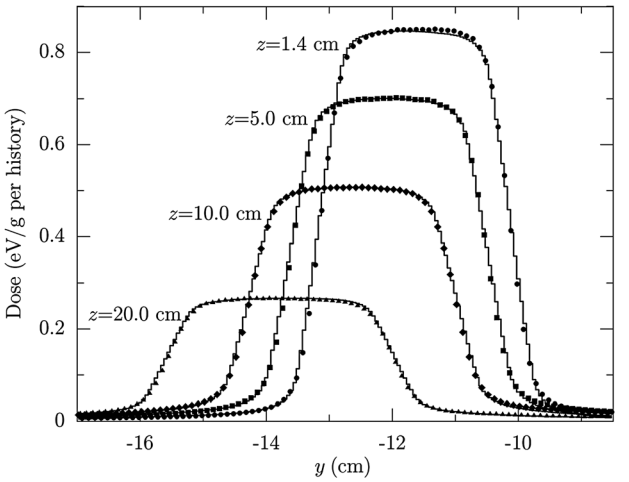

FIG. 8. Lateral profiles at different depths z obtained when the x coordinate is kept constant at 4.5 cm (center of the field). Irradiation conditions and other details are the same as in Fig. 6.

When more demanding criteria to the gamma test are set, those of 1% dose difference and a DTA of 0.1 cm, the results obtained are $\gamma_1 = 0.7\%$ and $\gamma_{1.2} = 0\%$. Clearly, these criteria are considerably more stringent than the 3% and 0.3 cm values generally accepted for clinical dose calculations.[36]

III.A Timings

A pertinent measure of simulation speed is the CPU time required to achieve a given average relative statistical uncertainty. The inverse of the product of this time and the uncertainty squared is known as the simulation efficiency.

Analysis of the contribution of the various VRTs to the improvement in simulation efficiency illustrates the importance of selecting the appropriate method. To assess this contribution, a PSF of the off-axis field discussed above was generated in each one of the following cases: (1) analogue simulation, i.e., without VRTs; (2) interaction forcing in the target; (3) interaction forcing in the target plus movable-skins; (4) same as (3) plus standard splitting with $K = 15$ replicas, a value derived after the work of Brualla and Sauerwein;[37] (5) same as (4) but using rotational splitting; (6) same as (4) but using fan splitting. The speedup, or increase in simulation efficiency, was evaluated using the latent variance[38] as a measure of the "uncertainty" of the PSF. The latent variance was defined as that associated with the dose in a layer of water located between 1.3 and 1.5 cm of depth, where the maximum lies. The results obtained, when case (1) is taken as the reference, are shown in table I. Note that for the case under study, fan splitting is about 17 times more efficient than rotational splitting and about 240 times more efficient than standard splitting.

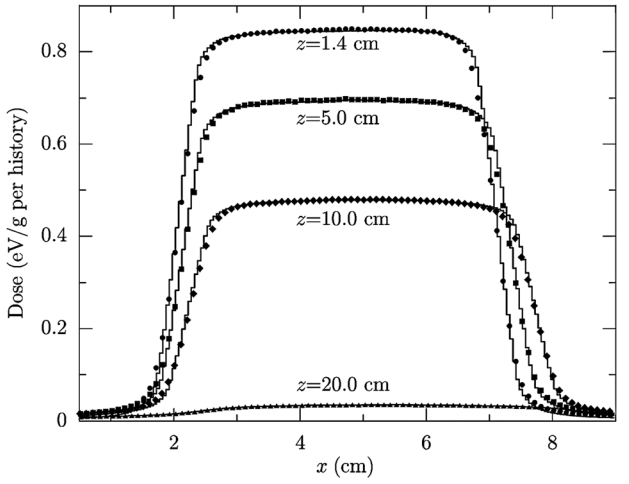

FIG. 7. Lateral profiles at different depths z obtained when the y coordinate is kept constant at -11.5 cm (center of the field). Irradiation conditions and other details are the same as in Fig. 6.

The codes were compiled with Intel Fortran for Mac OS X and run on a single core of a 2.8 GHz Intel Core 2 Duo processor. By default, interaction forcing, movable-skins and fan splitting (case 6 in Table I) are always used. Note, however, that when the field contains the central axis, as in the case of the 40×40 cm^2 reference field, rotational splitting is applied—see Sec. II A. Under these conditions, the computation of the dose distribution for the off-axis case with voxels of $2.5 \times 2.5 \times 2.5$ mm^3 and with an average standard statistical uncertainty of 2% (1σ), can be obtained in 3.1 h.

TABLE I. Increase in simulation efficiency (rounded to, at most, two significant digits) of the off-axis field for various VRTs, relative to the case of an analogue simulation. Additional details on these VRTs are given in the text.

Case	Variance-reduction technique	Speedup
1	No variance-reduction	$\equiv$ 1 (reference)
2	Interaction forcing	2
3	IF & movable-skins	5
4	IF & MS & standard splitting	7
5	IF & MS & rotational splitting	100
6	IF & MS & fan splitting	1700

IV. DISCUSSION AND CONCLUSIONS

The excellent agreement between simulation and experiment presented in the Sec. III indicates that detailed modeling of the linac geometry, the applied VRTs and the selected transport parameters are valid. However, simulation accuracy is only one of the relevant aspects. Since greater detail and accuracy usually imply more computation, another critical feature is simulation speed, which determines whether or not the code is of practical value. The far-from-axis field presented in this work is, in this respect, an extreme case that puts the code to the test. The goal was therefore to achieve reasonably low computing times for this challenging problem.

Table I demonstrates that fan splitting, the new VRT introduced in Sec. II A, is crucial to achieve this goal. Indeed, computation of the dose distribution in the water phantom for the off-axis case, which takes 3.1 h with the current version of PENEASYLINAC running on a single CPU core, would take about a month if standard splitting had been employed, or over 7 months in the case of an analogue simulation.

Notice that the uncertainty associated with the mean dose per history depends on voxel size; consequently, the time needed to achieve a given uncertainty also depends on this size. It can be seen that the CPU time is approximately inversely proportional to voxel area.[39] Hence, the time reported above would be further reduced if less spatial resolution is requested, as is usually the case in most treatment planning systems, where 2–5 mm voxels are common.

In summary, the two new PENELOPE-based MC simulation tools presented here, PENEASY and PENEASYLINAC, can simulate Varian Clinacs of the 600, 1800, 2100, and 2300 series, including their electron applicators and MLCs, in both an accurate and efficient manner. The modular structure of PENEASY allows the development of new tallies, source models and VRTs that extent the capabilities of the code to cover more specific needs. Thus, an auxiliary module written in C++ by I. Martínez-Rovira and collaborators[40] allows reading and writing of PSFs in the standardized binary format defined by the IAEA.[41] Furthermore, an extension for medical imaging systems has been developed by Badal.[42] Others extensions are under development. Along these lines, we would like to mention the work to include Elekta[43] linacs and to develop a graphical interface, called PRIMO, which will facilitate input from the user. PENEASYLINAC will be made publicly available in the near future by the authors.

ACKNOWLEDGMENTS

We thank Miguel L. Rodríguez, from the Centro Médico Paitilla (Panama), for providing the experimental measurements. We acknowledge partial financial support from the Spanish Ministerio de Ciencia e Innovación, Project No. FPA2009-14091-C02-01, and from the Networking Research Center on Bioengineering, Biomaterials and Nanomedicine (CIBER-BBN), Barcelona, Spain.

[a]Electronic mail: josep.sempau@upc.es

[1]Ma, C.-M. and S. B. Jiang, "Monte Carlo modelling of electron beams from medical accelerators," Phys. Med. Biol. **44**, R157–R189 (1999).
[2]F. Verhaegen and J. Seuntjens, "Monte Carlo modelling of external radiotherapy photon beams," Phys. Med. Biol. **48**, R107–R164 (2003).
[3]A. F. Bielajew and D. W. O. Rogers, "Variance-reduction techniques," *Monte Carlo Transport of Electrons and Photons*, T. M. Jenkins, W. R. Nelson, A. Rindi, A. E. Nahum, and D. W. O. Rogers eds., Plenum, New York (1988), pp. 407–419.
[4]R. Y. Rubinstein, *Simulation and the Monte Carlo Method* (John Wiley and Sons, New York, 1981).
[5]O. Chibani and C.-M. C. Ma, "On the discrepancies between Monte Carlo dose calculations and measurements for the 18 MV Varian photon beam," Med. Phys. **34**, 1206–1216 (2007).
[6]D. W. O. Rogers, B. A. Faddegon, G. X. Ding, C.-M. Ma, J. We, and T. R. Mackie, "BEAM: A Monte Carlo code to simulate radiotherapy treatment units," Med. Phys. **22**, 503–524 (1995).
[7]D. W. O. Rogers, B. Walters, and I. Kawrakow, "BEAMnrc Users Manual. Technical Report No. PIRS-0509(A)revK, National Research Council of Canada (2007).
[8]W. R. Nelson, H. Hirayama, and D. W. O. Rogers, "The EGS4 Code System. Technical Report No. SLAC-265 (Stanford Linear Accelerator Center, Stanford, California, 1985).
[9]I. Kawrakow, "Accurate condensed history Monte Carlo simulation of electron transport. I. EGSnrc, the new EGS4 version," Med. Phys. **27**, 485–498 (2000).
[10]I. Kawrakow, E. Mainegra-Hing, D. W. O. Rogers, F. Tessier, and B. R. B. Walters, "The EGSnrc code system: Monte Carlo simulation of electron and photon transport," Technical Report No. PIRS-701, National Research Council of Canada (2010).
[11]Note 1. Varian Medical Systems, Palo Alto, CA.
[12]F. Salvat, J. M. Fernández-Varea, and J. Sempau, "PENELOPE-*2008: A Code System for Monte Carlo Simulation of Electron and Photon Transport*," Issy-les-Moulineaux, France: OECD Nuclear Energy Agency (2009). Available in pdf format at http://www.nea.fr.
[13]J. Sempau, E. Acosta, J. Baró, J. M. Fernández-Varea, and F. Salvat, "An algorithm for Monte Carlo simulation of coupled electron-photon transport," Nucl. Instrum. Methods B **132**, 377–390 (1997).
[14]R. Alfonso, P. Andreo, R. Capote, M. S. Huq, W. Kilby, P. Kjäll, T. R. Mackie, H. Palmans, K. Rosser, J. Seuntjens, W. Ullrich, and S. Vatnitsky, "A new formalism for reference dosimetry of small and nonstandard fields," Med. Phys. **35**, 5179–5186 (2008).
[15]Note 2. http://www.upc.es/inte/downloads/penEasy.htm.
[16]A. E. Nahum, "Water/air stopping power ratios for megavoltage photon and electron beams," Phys. Med. Biol. **23**, 24–38 (1978).
[17]L. Brualla, F. Salvat, and R. Palanco-Zamora, "Efficient Monte Carlo simulation of multileaf collimators using geometry-related variance-reduction techniques," Phys. Med. Biol. **54**, 4131–4149 (2009).
[18]V. Panettieri, P. Barsoum, M. Westermark, L. Brualla, and I. Lax, "AAA and PBC calculation accuracy in the surface build-up region in tangential beam treatments. Phantom and breast case study with the Monte Carlo code PENELOPE," Radiother. Oncol. 93, 94–101 (2009).
[19]K. Bush, S. F. Zavgorodni, and W. A. Beckham, "Azimuthal particle redistribution for the reduction of latent phase-space variance in Monte Carlo simulations," Phys. Med. Biol. **52**, 4345–4360 (2007).
[20]A. Badal and J. Sempau, "A package of Linux scripts for the parallelization of Monte Carlo simulations," Comput. Phys. Commun. **175**, 440–450 (2006).
[21]N. Reynaert, S. C. van der Marck, D. R. Schaart, W. V. der Zee, C. V. Vliet-Vroegindeweij, M. Tomsej, J. Jansen, B. Heijmen, M. Coghe, and C. D. Wagter, "Monte Carlo treatment planning for photon and electron beams," Radiat. Phys. Chem. **76**, 643–686 (2007).
[22]W. Schneider, T. Bortfeld, and W. Schlegel, "Correlation between CT numbers and tissue parameters needed for Monte Carlo simulations of clinical dose distributions," Phys. Med. Biol. **45**, 459–478 (2000).
[23]Schaart, D. R., J. T. M. Jansen, J. Zoetelief, and P. F. A. de Leege, "A comparison of MCNP4C electron transport with ITS 3.0 and experiment at incident energies between 100 keV and 20 MeV: influence of voxel size, substeps and energy indexing algorithm," Phys. Med. Biol. **47**, 1459–1484 (2002).
[24]B. R. B. Walters and I. Kawrakow, "A "HOWFARLESS" option to increase efficiency of homogeneous phantom calculations with DOSXYZnrc," Med. Phys. **34**, 3794–3807 (2007).
[25]J. Sempau, S. J. Wilderman, and A. F. Bielajew, "DPM, a fast, accurate Monte Carlo code optimized for photon and electron radiotherapy treatment planning dose calculations," Phys. Med. Biol. **45**, 2263–2291 (2000).

[26]J. Amanatides and A. Woo, "A fast voxel traversal algorithm for ray tracing," *Eurographics'87* (Elsevier Science Publishers, Amsterdam, North-Holland, 1987), pp. 3–10.
[27]ICRU, "Stopping powers for electrons and positrons," Technical Report No. 37 (ICRU, Bethesda MD, 1984).
[28]E. García, J. Jiménez, and J. Puimedón, "Dose calculation in patients with PENELOPE/PENGEOM," J. Phys.: Conf. Series **74**, 012006 (2007).
[29]V. Moskvin and L. Papiez, "Voxel PENELOPE for radiation therapy applications," in Proceedings of MC2005, American Nuclear Society Topical Meeting in Monte Carlo, Chattanooga, TN, April 17–21 (2005). Available online from http://rsicc.ornl.gov/rsiccnew/MC2005_Presentations/MoskvinPresentation.pps.
[30]V. Taranenko and M. Zankl, Photon and electron transport simulation in voxel geometry with PENELOPE," Biomed. Tech. 50 suppl. **1**, 271–272 (2005).
[31]Note 3. PTW Freiburg GmbH, Germany.
[32]D. W. O. Rogers and R. Mohan, "Questions for comparison of clinical Monte Carlo codes, in W. Schlegel and T. Bortfeld, eds., *Proceedings of the XIII'th Conference on the Use of Computers in Radiation Therapy*, Heidelberg, Germany, pp. 120–122 Springer (2000).
[33]P. Andreo, D. T. Burns, K. Hohlfeld, M. S. Huq, T. Kanai, F. Laitano, V. Smyth, and S. Vynckier, "Absorbed dose determination in external beam radiotherapy: An international code of practice for dosimetry based on standards of absorbed dose to water," Technical Report No. TRS 398, (International Atomic Energy Agency, Vienna, Austria, 2000).
[34]D. A. Low, W. B. Harms, S. Mutic, and J. A. Purdy, "A technique for the quantitative evaluation of dose distributions," Med. Phys. **25**, 656–661 (1998).
[35]Note 4. The term history is used here to denote a primary electron impinging on the target and all the secondary particles produced by it.
[36]D. A. Low and J. F. Dempsey, "Evaluation of the gamma dose distribution comparison method," Med. Phys. **30**, 2455–2464 (2003).
[37]L. Brualla and W. Sauerwein, "On the efficiency of azimuthal and rotational splitting for Monte Carlo simulation of clinical linear accelerators," Radiat. Phys. Chem. **79**, 929–932 (2010).
[38]J. Sempau, A. Sánchez-Reyes, F. Salvat, H. O. ben Tahar, S. B. Jiang, and J. M. Fernández-Varea, "Monte Carlo simulation of electrons beams from an accelerator head using PENELOPE," Phys. Med. Biol. **46**, 1163–1186 (2001).
[39]J. Sempau and A. F. Bielajew, "Towards the elimination of Monte Carlo statistical fluctuation from dose volume histograms for radiotherapy treatment planning," Phys. Med. Biol. **45**, 131–157 (2000).
[40]Note 5. http://www.upc.es/inte/downloads/penEasy_IAEAaddon.htm.
[41]R. Capote, R. Jeraj, C.-M. Ma, D. W. O. Rogers, F. Sánchez-Doblado, J. Sempau, J. Seuntjens, and J. V. Siebers, "Phase-space database for external beam radiotherapy," Technical Report No. INDC(NDS)-0484 (International Atomic Energy Agency, Nuclear Data Section, Vienna, Austria, 2006).
[42]Note 6. http://code.google.com/p/peneasy-imaging.
[43]Note 7. Elekta Ltd., West Sussex, UK.